ARTICLE

Challenges in the synthesis of corannulene-based non-planar nanographenes on the Au(111) surfaces

Tao Wang,[*a,b] James Lawrence,[a,b] Naoya Sumi,[a,b] Roberto Robles,[a] Jesus Castro-Esteban,[c] Dulce Rey,[c] Mohammed S. G. Mohammed,[a,b] Alejandro Berdonces-Layunta,[a,b] Nicolas Lorente,[a,b] Dolores Pérez,[c] Diego Peña,[*c] Martina Corso,[*a,b] and Dimas G. de Oteyza[a,b,e]

The synthesis of non-planar nanographenes on surfaces is a challenging task. Herein, with the aid of bond-resolving scanning tunneling microscopy (BRSTM) and density functional theory (DFT) calculations, we present a systematic study aiming at the fabrication of corannulene-based nanographenes *via* intramolecular cyclodehydrogenations on a Au(111) surface. The formation of the non-planar targeted products is confirmed to be energetically unfavored compared to the formaiton of planar/quasi-planar undesired competing monomer products. In addition, the activation of intermolecular coupling furhter inhibits formation of the final targeted product. Although it was not possible to access the corannulene moiety by means of on-surface synthesis, partial cyclodehydrogenation of the molecular precursors was demonstrated.

Introduction

Owing to their unparalleled optoelectronic and magnetic properties, nanographenes have attracted intensive attention of a broad scientific community.[1-3] In particular, "on-surface synthesis (OSS)" under ultrahigh vacuum (UHV) conditions offers an unprecedented opportunity for the precise synthesis and characterization of nanographenes on surfaces.[4-7] The formation of targeted planar π-conjugated nanographenes often involves intramolecular cyclodehydrogenations whose occurrence is typically promoted by the two-dimensional (2D) surface.[8, 9] Therefore, several planar products which are difficult to synthesize by solution-phase chemistry have been successfully obtained on surfaces by surface-assisted planarization[8, 10] or even carbon bond rearrangements.[11]

However, compared to the success of the synthesis of planar nanographenes, the fabrication of non-planar bowl-shaped nanographenes *via* OSS approach is much more challenging and only few examples thereof have been reported.[12-15] Those examples were achieved by using either highly reactive Pt(111) as the substrate or nitrogen doped molecules as the precursors. However, the strong substrate-molecule interaction impedes the decoupling of nanographene from the surface. It also hampers the controllable molecular manipulation by a scanning probe or light excitation, as required e.g. with molecule-based nano-machines.[16] Besides, the solution-based synthesis of non-planar pure hydrocarbon molecules like corannulene is normally time consuming and expensive,[17] making an alternative OSS strategy from easily available starting materials highly desirable. There are thus good reasons to motivate the development of strategies that allow synthesizing non-planar nanographenes composed of pure hydrocarbon on a Au(111) surface.

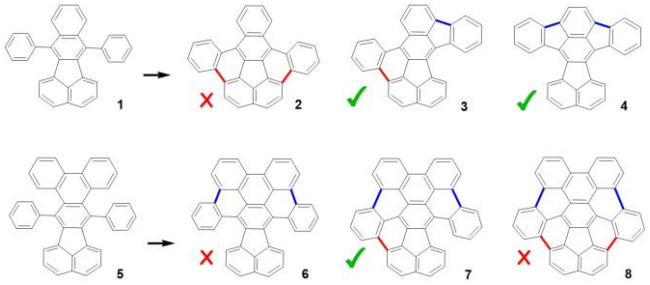

Scheme 1 Possible products generated *via* the intramolecular cyclodehydrogenation from precursor **1** and **5**. The formed covalent bonds are denoted by either red (for the formation of corannulene unit) or blue lines. The experimentally observed and missing products are marked by green checkmarks and red crosses, respectively.

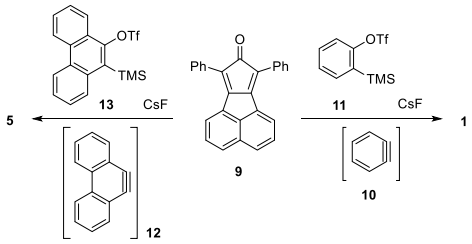

Scheme 2 Synthesis of precursors **1** and **5**.

[a] Donostia International Physics Center, San Sebastián, 20018, Spain. E-mail: taowang@dipc.org, martina.corso@ehu.eus
[b] Centro de Fisica de Materiales, CSIC-UPV/EHU, San Sebastián, 20018, Spain.
[c] Centro Singular de Investigación en Química Biolóxica e Materiais Moleculares (CiQUS) and Departamento de Química Orgánica, Universidade de Santiago de Compostela, Santiago de Compostela, 15782, Spain. E-mail: diego.pena@usc.es
[d] Ikerbasque, Basque Foundation for Science, Bilbao, 48013, Spain.

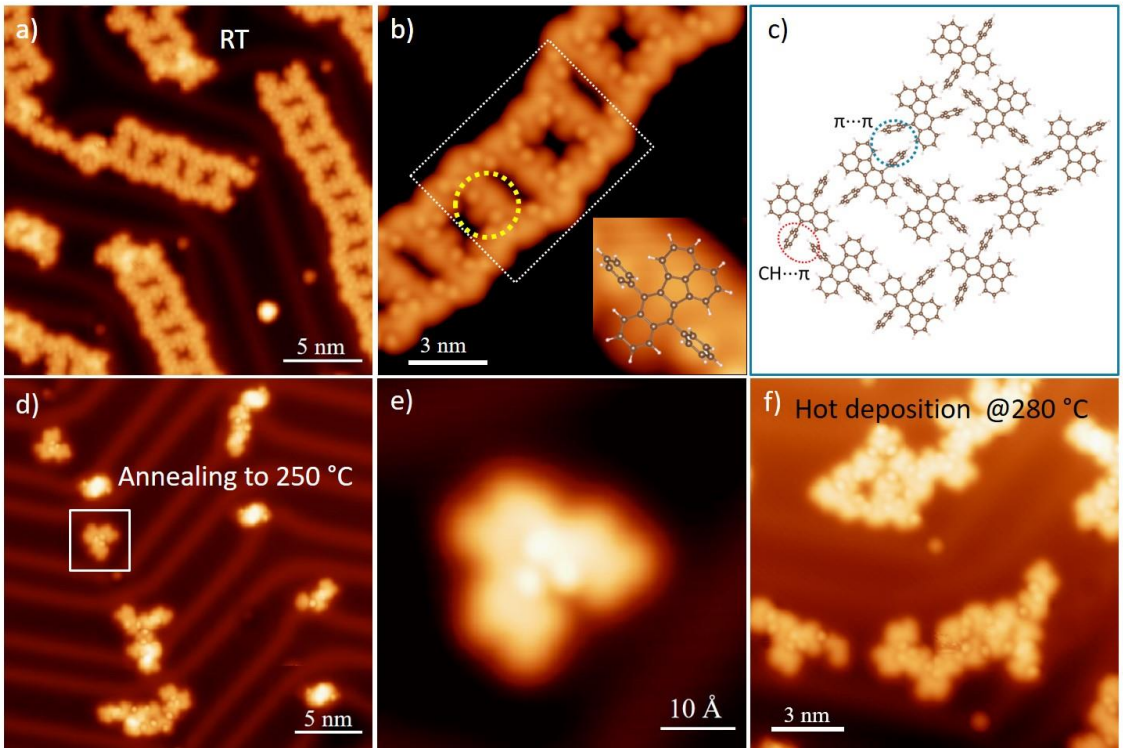

Fig. 1 (a,b) Overview and magnified STM images of the sample prepared by depositing molecule **1** on Au(111) held at RT, respectively. A monomer in the self-assembled structure is marked by a yellow circle in (b). A molecular model is overlaid on the zoom-in STM image of the yellow dotted monomer, as shown in the inset. (c) Molecular models revealing the white framed region in (b). Examples of π···π and CH···π intermolecular interactions are marked by blue and red dotted circles, respectively. (d) Overview STM image recorded after annealing the as-prepared sample to 250 °C. (e) Zoom-in STM image of the white framed region in (d). (f) Overview STM image obtained on the sample by deposition of molecule **1** on Au(111) held at 280 °C. Scanning parameters: (a,f) U=1 V, I=100 pA; (b) U=500 mV, I=100 pA; (d,e) U=−500 mV, I=−100 pA. Color code for molecular models: C, gray; H, white.

Herein, our study is focused on the synthesis of non-planar nanographenes based on the well-known and popular corannulene molecule (a fragment of fullerenes).[18-20] With the combination of BRSTM and DFT calculations, we have investigated two on-surface reactions aiming at the fabrication of corannulene-based non-planar nanographenes on Au(111). Compounds **1** and **5** (Scheme 1) are used as the precursors. The potential products expected from cyclodehydrogenation reactions (**2**-**4**, **6**-**8**) are shown in Scheme 1. The results indicate that both precursors are inadequate for the synthesis of corannulene-based nanographenes **2** and **8** on Au(111). The experimentally observed products (**3**, **4**, **7**) are marked by green checkmarks in Scheme 1. We attribute the lack of success in the synthesis of **2** and **8** to the following reasons:
i) for the reaction of molecule **1**, the formation of planar/*quasi*-planar structures (**3**, **4**) is energetically favored with respect to corannulene-based non-planar structure **2**; and ii) for the reaction of molecule **5**, the activation of intermolecular coupling reactions between intermediate products **7** at high surface temperatures proceeds before formation of the final product **8**. Nevertheless, in spite of failing its original goal, this study provides key insight into the reaction processes during the fabrication of targeted corannulene-based nanographenes on surfaces, thus providing valuable guidance for optimizing the precursor and reaction strategy in the future.

Experimental

1. STM measurement

All LT-STM experiments were performed using a commercial Scienta-Omicron LT-STM, cooled to 4.3 K. A single crystal Au(111) (MaTeck) was used for all experiments. The crystal was cleaned *via* cycles of argon sputtering and annealing up to 450 °C . The sublimation temperatures of molecules **1** and **5** were 155 °C and 200 °C, respectively. The deposition time was 5 minutes for the samples prepared at RT. CO was deposited onto the sample *via* a leak valve at a pressure of approximately 5×10^{-9} mbar and a maximum sample temperature of 7.0 K. CO is usually imaged as a depression on the Au(111) surface, and can be picked up with a metallic tip when scanning over it or by applying a −2 V bias voltage pulse when the tip is in typical tunneling conditions (*e.g.* I=100 pA, U=0.5 V).

2. DFT calculation

Ab initio calculations were performed in the framework of the density functional theory (DFT) as implemented in VASP.[21] GGA in the PBE flavor was used for the exchange and correlation

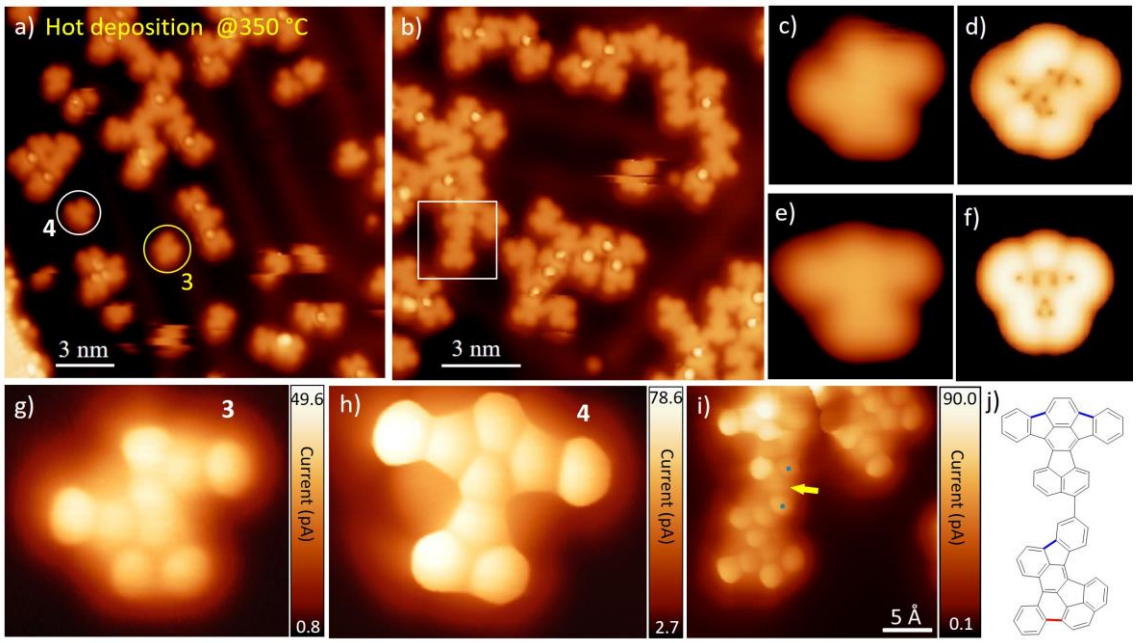

Fig. 2 (a,b) STM images of the sample prepared by depositing precursor **1** on Au(111) held at 350 °C. (c,d) Conventional experimental and simulated (at -1.5 V) STM image of product **3**. (e,f) Conventional experimental and simulated (at -1.5 V) STM image of product **4**. (g,h) Representative bond-resolving STM images of products **3** and **4**, respectively, recorded by CO-functionalized probes. (i) Zoom-in STM image of the white framed region of (b) with a CO-functionalized probe. (j) Molecular structure of the polymer in (i). Scanning parameters: (a) U=−1 V, I=−40 pA; (b) U=−1 V, I=−90 pA; (c,e) U=−1.2 V, I=−50 pA (g,h,i) U=2 mV.

functional.[22] Wavefunctions were expanded using a plane wave basis set with an energy cut-off of 500 eV. Core electrons were treated using PAW potentials.[23, 24] A big unit cell of 50x40x30 Å^3 was used to avoid interactions between periodic replicas. Geometries were optimized until all the forces were smaller than 0.01 eV/Å. STM simulations were performed in the Tersoff-Hamann approximation[25] following the method of Bocquet *et al.*[26] as implemented in the STMpw program.[27]

Results and discussion

Precursor synthesis

Compounds **1** and **5** were easily obtained by means of aryne chemistry in one step from cyclopentadienone **9** (Scheme 2).[28] In particular, reaction of **9** with benzyne (**10**), which was *in situ* generated by fluoride-induced decomposition of triflate **11**, led to the formation of compound **1** in 97% yield, in a sequence of a Diels-Alder reaction followed by CO extrusion. Similarly, reaction of **9** with 9,10-phenanthryne (**12**), which was generated by reaction of triflate **13** with CsF, afforded compound **5** in 86% yield (see ESI for details).†

On-surface reactions of molecule 1

Fig. 1a displays a representative STM image of the sample prepared by depositing precursor molecule **1** on Au(111) held at room temperature (RT). It shows that the monomers self-assemble into ladder-like supramolecular structures. A monomer **1** is marked by the yellow dotted circle in the magnified high-resolution STM image in Fig. 1b. The two phenyl groups, which connect with the molecular backbone through σ-bonds, exhibit bright features due to their non-planar adsorption configurations.[29-31] A molecular model is overlaid on the zoom-in STM image of the monomer displayed in the inset of Fig. 1b. The optimized molecular structure of **1** by gas-phase DFT calculation is shown in Fig. S1 along with the rest of structures **1**-**8**. CH···π[32] and π···π[33, 34] intermolecular interactions are presumably involved in the stabilization of the ladder-like self-assembled structure, as revealed by the molecular models exhibited in Fig. 1c. The STM image in Fig. 1b overlaid with the molecular models is shown in Fig. S2.

Next, the sample was annealed to 250 °C to trigger the intramolecular cyclodehydrogenations of **1**. As shown in Fig. 1d and 1e, only one intramolecular cyclodehydrogenation reaction takes place on **1**, while the second phenyl remains unreacted and non-planar (bright dots in Fig. 1e). In addition, a dramatic molecular desorption takes place during the annealing treatment. Only few molecules remain adsorbed, typically at the corners of the herringbone reconstruction (Fig. 1d), hindering a potential annealing treatment at higher temperature that could drive the planarization of the second phenyl unit as well. Alternatively, we tried depositing molecule **1** on the preheated Au(111) surface at 280 °C with a longer evaporation time (10 mins *vs.* 5 mins) to avoid the molecular desorption during the annealing. However, as in the post-annealing procedure, most of the products still present three-dimensional morphologies (Fig. 1f).

Aiming at the activation of the second intramolecular cyclodehydrogenation of **1**, we followed the same procedure at

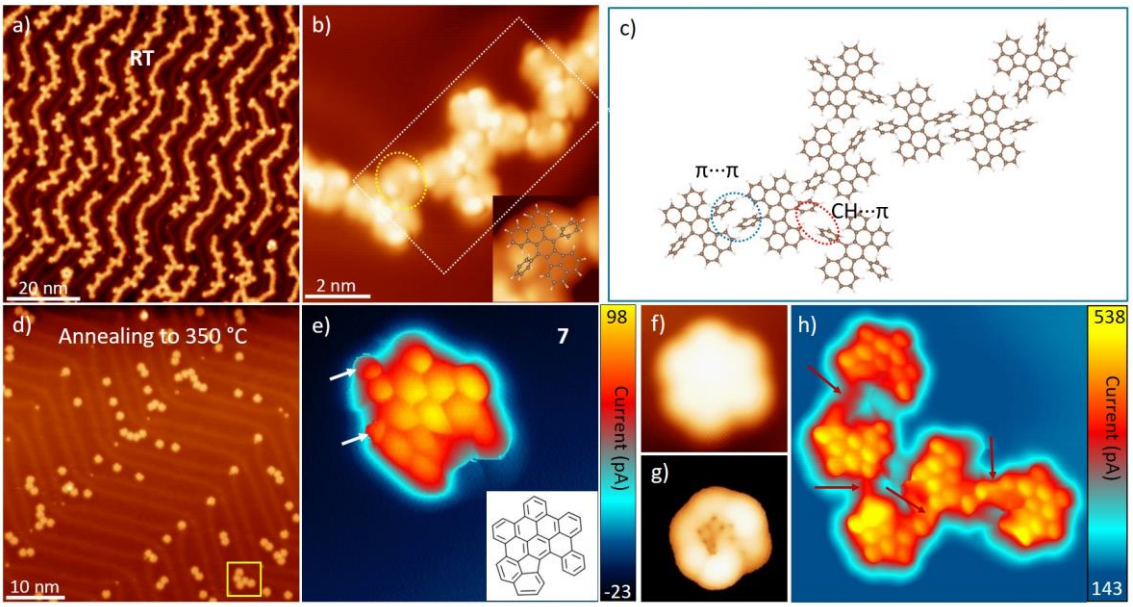

Fig. 3 (a) Overview STM image of the sample prepared by depositing precursor molecule **5** on Au(111) at RT. (b) A typical magnified STM image of the snake-like self-assembly structure formed at RT. A monomer is marked by a yellow dotted circle. A molecular model is overlaid on the zoom-in STM image of the yellow dots circled monomer, as shown in the inset. (c) Molecular models revealing the white framed region in (b). Examples of π···π and CH···π intermolecular interactions are marked by blue and red dotted circles, respectively. (d) Overview STM image recorded after annealing the as-prepared sample to 350 °C. (e) Representative constant height bond-resolving STM image of the isolated monomer in (d) using a CO-functionalized probe. The two small protrusions caused by movement of molecule **7** are marked by white arrows. The chemical structure of product **7** are inserted at the right bottom corner. (f) STM image recorded by conventional scanning parameters. (g) Simulated STM image using at -1.5 V. (h) Bond-resolving STM image of the yellow framed region in (d), using a CO-functionalized probe. Scanning parameters: (a) U=−500 mV, I=−50 pA; (b) U=−500 mV, I=−100 pA; (d) U=500 mV, I=100 pA; (e) U=5 mV; (f) U=−1 V, I=−60 pA; (h) U=10 mV.

an even higher temperature. That is, molecule **1** was deposited on the Au(111) surface held at a temperature of 350 °C. A sample with ~0.3 monolayer (ML) molecular coverage was obtained, as shown in Fig. 2a and 2b. Apart from disordered polymeric structures, two different single-molecule products are formed *via* intramolecular cyclodehydrogenations of **1**, as marked by yellow and white circles, respectively. Both of them display an almost planar adsorption configuration on Au(111). One is asymmetric, while the second one is axisymmetric (Fig. 2c-f). The constant height bond-resolving STM images recorded with CO functionalized probes,[35] as shown in Fig. 2g and 2h, reveal that the two different products are assigned to products **3** and **4** (Scheme 1), respectively. One five- and one six-membered rings are generated for the formation of **3** while two five-membered rings are created for the formation of **4**. The ratio between **3** and **4** is approximately 1:1 (a statistical analysis is show in Fig. S3). However, most of the molecules do not remain as single molecules but form covalent polymers, as displayed in the overview STM images. While many of the phenyl moieties remain non-planar (corresponding to the brighter dots along the polymer structures), there are considerable polymer segments that appear planarized, *e.g.* the white framed region in Fig. 2b. The zoom-in bond-resolving STM image of this region (Fig. 2i) reveals that the chain-like structure is generated from the coupling between **3** and **4** *via* a σ-bond (pointed by a yellow arrow). A non-covalent assembly can be excluded from the short center-to-center distance between the two six-membered rings (blue dots in Fig. 2i), which is in the range of 4.1-4.3 Å and thus necessarily implies a covalent coupling.[29, 36] The corresponding chemical structure is shown in Fig. 2j. We thus conclude that the reaction pathway involved in the intermolecular coupling between monomers is readily activated at 350 °C, leading to the formation of various covalent polymers.

The targeted corannulene-based product **2** was not observed on the sample. This indicates that the formations of the planar (or *quas*i-planar) products **3** and **4** are energetically favored with respect to the non-planar product **2**. In addition, a following intramolecular cyclodehydrogenation of **3** and **4** to form a corannulene-based product is extremely difficult due to the large distance between the two corresponding phenyl groups. Instead, the C-H bond activation of products **3** and **4** leading to intermolecular coupling reactions is obviously preferred at high surface temperatures, forming covalent disordered polymers.

On-surface reactions of molecule 5

In order to facilitate the reaction toward the formation of corannulene-based structures, an alternative precursor was synthesized (molecule **5** in Scheme 1). A stepwise cyclodehydrogenation reaction (**5**→**6**→**7**→**8**) can be expected on such molecular structure. Figure 3a displays an overview STM image of the Au(111) surface after deposition of molecule **5** at RT. Snake-like self-assembled structures were obtained. As

Potential product	2	3	4	6	7	8
Formation energy/eV	1.63	0.98	1.47	−0.06	0.15	1.18

Table 1 Formation energies for the potential products listed in Scheme 1.

shown in the magnified STM image in Fig. 3b, similar to the case of molecule **1**, the two non-planar phenyl groups also exhibit bright features in this supramolecular structure. As a guide to the eye, a single molecule is marked by the yellow dotted circle in Fig. 3b, within which two bright sections corresponding to the non-planar phenyl units can be distinguished on either side. A molecular model is overlaid on the zoom-in STM image of the monomer, as shown in the inset. Also here, π···π and CH···π intermolecular interactions are presumably the main stabilizing interactions of the self-assembled structure, as revealed by the molecular models shown in Fig. 3c. The STM image in Fig. 3b overlaid with the molecular models is shown in Fig. S4.

Annealing the sample to 350 °C activates the intramolecular cyclodehydrogenation reaction of **5**. As shown in the overview STM image in Fig. 3d, many *quasi*-planar products displaying the same morphology are observed. Figure 3e shows a typical bond-resolving STM image of the product using a CO-functionalized probe. It reveals that the product corresponds to molecule **7** in Scheme 1. The observation of the two small additional protrusions (pointed by white arrows) in the STM image is attributed to the slight movement of molecule **7** at the short tip-sample distances utilized. The repulsive interaction between **7** and the probe easily induces the molecular movement, especially because the product **7** is not completely planar (Fig. S1). This is confirmed by the experimental fact that the additional small protrusions were not observed in the STM image of the same molecule by using conventional scanning parameters (Fig. 3f; U=−1 V, I=−60 pA) at which the probe is comparatively far from the molecule. This conventional STM image matches well with the simulated one (Fig. 3g).

The targeted corannulene-based product **8** was still not observed on the sample. Instead, intermolecular coupling between several compounds was readily activated at 350 °C. For example, the yellow framed region in Fig. 3d contains a covalent pentamer formed by the C–C couplings between five products **7**. The magnified bond-resolving STM image of the covalent pentamer is shown in Fig. 3h. These observations imply that the intermolecular coupling between molecules **7** occurs prior to the intramolecular cyclodehydrogenation of **7** on Au(111).

We also tried depositing molecule **5** on a hot Au(111) surface held at 400 °C to trigger the reaction. This leads to a similar result as the experiment of RT deposition followed by 350 °C annealing and no targeted product **8** was observed either (Fig. S5).

All the experimental results above reveal that precursors **1** and **5** follow energetically unfavourable reaction pathways unsuitable for the OSS of corannulene-based non-planar nanographenes. On the one hand, the formation of relatively planar products is favored with respect to that of corannulene-based structures. On the other hand, the activation of intermolecular coupling at high surface temperatures further increases the difficulty for the formation of corannulene moieties (the last missing bond).

DFT calculations

In the following, gas-phase DFT-based thermodynamic calculations were performed to gain a further insight into the various intramolecular reaction pathways of **1** and **5** on Au(111). The formation energy of each product in the electronic enthalpy path can be calculated using the energy of the product plus the energy of combinatively desorbed H_2 minus the energy of the precursor. The results are listed in Table 1. It can be seen that the majority of products have positive formation energies in the electronic enthalpy path. However, note that multiple reactions under UHV have been reported to occur in spite of an increasing enthalpy,[37-39] which are driven by the overall free energy decrease from the increased entropy of the liberated hydrogen.[40, 41] For the reaction of precursor **1**, the formation energy of corannulene-based product **2** is higher than those of the other two planar/*quasi*-planar products **3** and **4** observed experimentally. In addition, the energy difference between planar and non-planar products will be larger if the Au(111) substrate is taken into account in the calculations due to the 2D confinement and the increased molecule-substrate interactions for planar adsorbates.[8] Therefore, it is not surprising that no corannulene-based product **2** was observed in the experiment. We note that the energy difference between **3** and **4** will decrease if the substrate is taken into calculation, since **3** is not completely planar either, thus explaining that both products were observed simultaneously and in comparable amounts.

As stated above, for the reaction of precursor **5**, products **6**, **7**, and **8** can be thought as formed stepwise. As shown in Table 1, corannulene-based product **8** has a much higher formation energy than **6** and **7**, thus its formation is thermodynamically unfavourable. In addition, as corroborated by the experiment, the activation of the intermolecular coupling also sets in prior to the formation of **8**. Those are reasons why no product **8** has been obtained in the experiments. We note that product **6** was also not observed in experiments. This may be attributed to a downhill diagram of the overall free energy from **6** to **7**. Since two atomic hydrogens were released in this step, the overall free energy may decrease from **6** to **7** due to the increased entropy of the liberated hydrogen as stated above. As a result, product **6** has a short lifetime and typically cannot be observed in experiments.

Discussion

Preliminary calculations on the formation energies of possible reaction products indicates that the precursors **1** and **5** are not good candidates to begin with. This is mostly because of two reasons: firstly, the formation of corannulene-based non-planar nanographenes is not energetically favored; secondly, the activation of intermolecular coupling between intermediates at high surface temperatures inhibits the formation of corannulene-based nanographenes. Based on these two points,

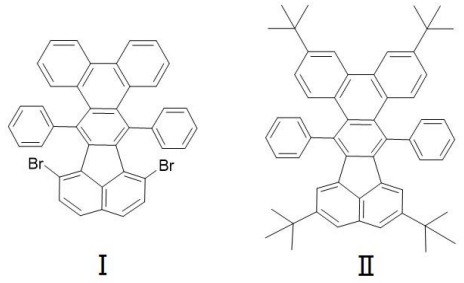

Fig. 4 Potential precursors for the synthesis of corannulene-based non-planar nanographenes on Au(111).

there are two solutions to promote the synthesis of the targeted products, either lowing the energy barrier or preventing the occurrence of intermolecular reactions. Therefore, here we propose two modified molecules as the potential candidates of the precursors (Fig. 4) for the synthesisof corannulene-based non-planar nanographenes in the future. For the case of molecule Ⅰ, the introduction of Br substituents may make the final cyclodehydrogenation easier, by directly generating two radicals after C-Br cleavage. For the case of molecule Ⅱ, the introduction of t-Butyl groups may hinder the intermolecular coupling by increasing the steric hindrance.

Conclusions

In conclusion, we have investigated the detailed intramolecular cyclodehydrogenation reaction pathways of two precursor molecules on a Au(111) surface upon thermal treatment. We find that the formation of the planar (or *quasi*-planar) structures are much more favourable than corannulene-based non-planar structures on Au(111). In addition, the activation of intermolecular coupling reactions at high surface temperatures also precedes the formation of corannulene-based products *via* intramolecular cyclodehydrogenation. Inspired by these findings, we propose two modified molecules as the potential precursors for the synthesis of corannulene-based non-planar nanographenes on Au(111). Nevertheless, how to rationally design precursor molecules and avoid the intermolecular couplings are still open questions for the synthesis of corannulene-based non-planar nanographenes on surfaces.

Author Contributions

Diego Peña, Nicolas Lorente, Martina Corso, and Dimas G. de Oteyza conceived the project. Tao Wang led the STM experiments together with James Lawrence, Naoya Sumi, Mohammed S. G. Mohammed, and Alejandro Berdonces-Layunta. Roberto Robles and Nicolas Lorente conducted the DFT calculation. The precursor molecules were synthesized by Jesus Castro-Esteban, Dulce Rey, under the guidance of Diego Peña and Dolores Pérez. The experimental data was analyzed by Tao Wang, James Lawrence, Naoya Sumi Martina Corso, and Dimas G. de Oteyza. The paper was written by Tao Wang, Roberto Robles, Jesus Castro-Esteban, and Dulce Rey, Diego Peña, Martina Corso, and Dimas G. de Oteyza.

Conflicts of interest

There are no conflicts to declare.

Acknowledgements

This work was financially supported by the Spanish Agencia Estatal de Investigación (PID2019-107338RB-C62 and PID2019-107338RB-C63 and MAT2016-78293-C6; AEI/FEDER, UE), the Basque Government (IT-1255-19), the European Union's Horizon 2020 Program (Grant No. 863098), the Xunta de Galicia (Centro singular de investigación de Galicia accreditation 2019-2022, ED431G 2019/03) and the European Union (European Regional Development Fund-ERDF). European Union's Horizon 2020 research and innovation programme under the project MEMO (Grant No. 766864).

Notes and references

1 I. Pozo, E. Guitián, D. Pérez and D. Peña, *Acc. Chem. Res.*, 2019, **52**, 2472.
2 A. Narita, X.-Y. Wang, X. Feng and K. Müllen, *Chem. Soc. Rev.*, 2015, **44**, 6616.
3 C. Wang, H. Dong, W. Hu, Y. Liu and D. Zhu, *Chem. Rev.*, 2012, **112**, 2208.
4 M. Treier, C. A. Pignedoli, T. Laino, R. Rieger, K. Müllen, D. Passerone and R. Fasel, *Nat. Chem.*, 2011, **3**, 61.
5 L. Grill, M. Dyer, L. Lafferentz, M. Persson, M. V. Peters and S. Hecht, *Nat. Nanotechnol.*, 2007, **2**, 687.
6 S. Clair and D. G. de Oteyza, *Chem. Rev.*, 2019, 119, 4717-4776.
7 T. Wang and J. Zhu, *Surf. Sci. Rep.*, 2019, **74**, 97.
8 Q. Zhong, Y. Hu, K. Niu, H. Zhang, B. Yang, D. Ebeling, J. Tschakert, T. Cheng, A. Schirmeisen, A. Narita, K. Müllen and L. Chi, *J. Am. Chem. Soc.*, 2019, **141**, 7399.
9 L. Feng, T. Wang, H. Jia, J. Huang, D. Han, W. Zhang, H. Ding, Q. Xu, P. Du and J. Zhu, *Chem. Commun.*, 2020, **56**, 4890.
10 R. Zuzak, J. Castro-Esteban, P. Brandimarte, M. Engelund, A. Cobas, P. Piatkowski, M. Kolmer, D. Perez, E. Guitian, M. Szymonski, D. Sanchez-Portal, S. Godlewski and D. Pena, *Chem. Commun.*, 2018, **54**, 10256.
11 T. G. Lohr, J. I. Urgel, K. Eimre, J. Liu, M. Di Giovannantonio, S. Mishra, R. Berger, P. Ruffieux, C. A. Pignedoli, R. Fasel and X. Feng, *J. Am. Chem. Soc.*, 2020, **142**, 13565.
12 S. Mishra, M. Krzeszewski, C. A. Pignedoli, P. Ruffieux, R. Fasel and D. T. Gryko, *Nat. Commun.*, 2018, **9**, 1714.
13 D. Skidin, F. Eisenhut, M. Richter, S. Nikipar, J. Krüger, D. A. Ryndyk, R. Berger, G. Cuniberti, X. Feng and F. Moresco, *Chem. Commun.*, 2019, **55**, 4731.
14 G. Otero, G. Biddau, C. Sánchez-Sánchez, R. Caillard, M. F. López, C. Rogero, F. J. Palomares, N. Cabello, M. A. Basanta and J. Ortega, *Nature*, 2008, **454**, 865.
15 J. R. Sanchez-Valencia, T. Dienel, O. Gröning, I. Shorubalko, A. Mueller, M. Jansen, K. Amsharov, P. Ruffieux and R. Fasel, *Nature*, 2014, **512**, 61.
16 Y. Shirai, A. J. Osgood, Y. Zhao, K. F. Kelly and J. M. Tour, *Nano Lett.*, 2005, **5**, 2330.
17 E. Nestoros and M. C. Stuparu, *Chem. Commun.*, 2018, **54**, 6503.

18 G. Povie, Y. Segawa, T. Nishihara, Y. Miyauchi and K. Itami, *Science*, 2017, **356**, 172.
19 L. T. Scott, M. M. Boorum, B. J. McMahon, S. Hagen, J. Mack, J. Blank, H. Wegner and A. de Meijere, *Science*, 2002, **295**, 1500.
20 E. M. Muzammil, D. Halilovic and M. C. Stuparu, *Commun. Chem.*, 2019, **2**, 58.
21 G. Kresse and J. Furthmüller, *Comput. Mat. Sci.*, 1996, **6**, 15.
22 J. P. Perdew, K. Burke and M. Ernzerhof, *Phys. Rev. Lett.*, 1996, **77**, 3865.
23 P. E. Blöchl, *Phys. Rev. B*, 1994, **50**, 17953.
24 G. Kresse and D. Joubert, *Phys. Rev. B*, 1999, **59**, 1758.
25 J. Tersoff and D. R. Hamann, *Phys. Rev. B*, 1985, **31**, 805.
26 M.-L. Bocquet, H. Lesnard, S. Monturet and N. Lorente, *Computational Methods in Catalysis and Materials Science*, Wiley-VCH Verlag GmbH & Co. KGaA, 2009, pp. 199–219.
27 N. Lorente and R. Robles, *STMpw*, 2019, https://zenodo.org/record/3581159.
28 D. Pérez, D. Peña and E. Guitián, Eur. *J. Org. Chem.*, 2013, **2013**, 5981-6013.
29 Q. Fan, D. Martin-Jimenez, S. Werner, D. Ebeling, T. Koehler, T. Vollgraff, J. Sundermeyer, W. Hieringer, A. Schirmeisen and J. M. Gottfried, *J. Am. Chem. Soc.*, 2020, **142**, 894.
30 D. G. de Oteyza, A. García-Lekue, M. Vilas-Varela, N. Merino-Díez, E. Carbonell-Sanromà, M. Corso, G. Vasseur, C. Rogero, E. Guitián, J. I. Pascual, J. E. Ortega, Y. Wakayama and D. Peña, *ACS Nano*, 2016, **10**, 9000.
31 J. Cai, P. Ruffieux, R. Jaafar, M. Bieri, T. Braun, S. Blankenburg, M. Muoth, A. P. Seitsonen, M. Saleh, X. Feng, K. Müllen and R. Fasel, *Nature*, 2010, **466**, 470.
32 Q. Li, C. Han, S. R. Horton, M. Fuentes-Cabrera, B. G. Sumpter, W. Lu, J. Bernholc, P. Maksymovych and M. Pan, *ACS Nano*, 2012, **6**, 566.
33 J. Hieulle, E. Carbonell-Sanromà, M. Vilas-Varela, A. Garcia-Lekue, E. Guitián, D. Peña and J. I. Pascual, *Nano Lett.*, 2018, **18**, 418.
34 T. Wang, Q. Fan, L. Feng, Z. Tao, J. Huang, H. Ju, Q. Xu, S. Hu and J. Zhu, *ChemPhysChem*, 2017, **18**, 3329.
35 P. Jelinek, *J. Phys. Conden.s Matter.*, 2017, **29**, 343002.
36 T. Wang, Y. Pan, W. Zhang, J. Lawrence, M. S. G. Mohammed, J. Huang, L. Feng, A. Berdonces-Layunta, D. Han, Q. Xu, X. Wu, S. L. Tait, D. G. de Oteyza and J. Zhu, *The J. Phys. Chem. Lett.*, 2020, **11**, 5902-5907.
37 Y. Q. Zhang, N. Kepčija, M. Kleinschrodt, K. Diller, S. Fischer, A. C. Papageorgiou, F. Allegretti, J. Björk, S. Klyatskaya, F. Klappenberger, M. Ruben and J. V. Barth, *Nat. Commun.*, 2012, **3**, 1286.
38 B. Cirera, N. Giménez-Agulló, J. Björk, F. Martínez-Peña, A. Martin-Jimenez, J. Rodriguez-Fernandez, A. M. Pizarro, R. Otero, J. M. Gallego, P. Ballester, J. R. Galan-Mascaros and D. Ecija, *Nat. Commun.*, 2016, **7**, 11002.
39 T. Wang, H. Lv, L. Feng, Z. Tao, J. Huang, Q. Fan, X. Wu and J. Zhu, *J. Phys. Chem. C*, 2018, **122**, 14537.
40 J. Björk, J. In *On-Surface Synthesis II*; Springer International Publishing, 2018; pp 19−34.
41 J. Björk, *J. Phys. Chem. C* 2016, **120**, 21716.

Electronic Supplementary Information

Calculations

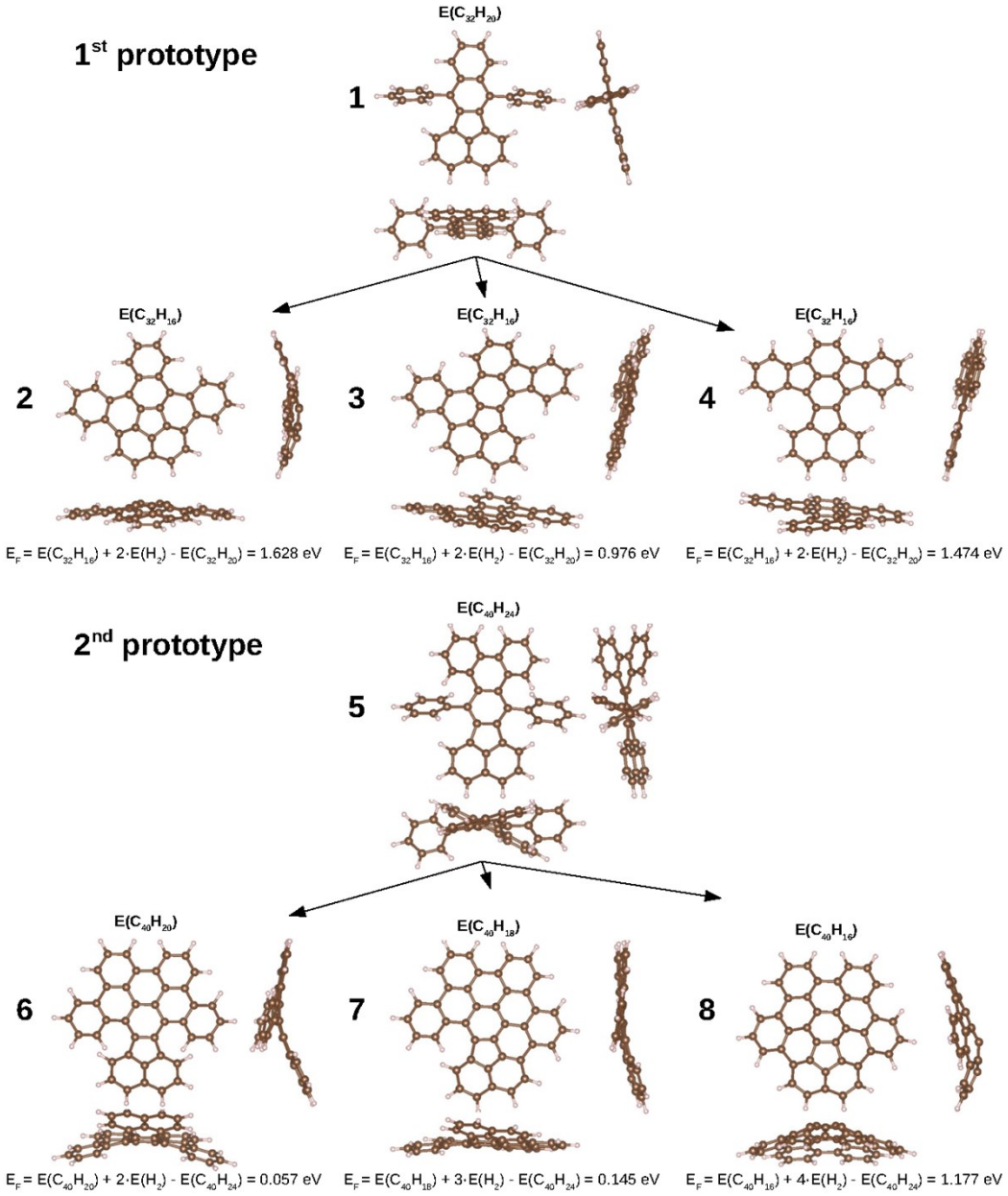

Fig. S1 DFT optimized molecular structures of the precursor and potential products in gas phase and the formation energies for all the products.

Additional STM images

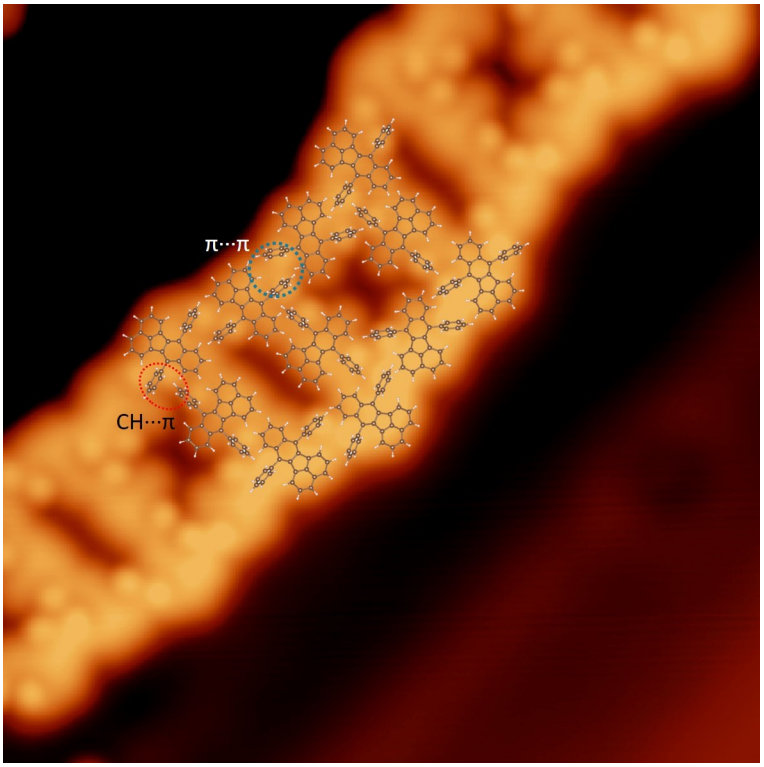

Fig. S2 STM image in Fig. 1b overlaid with the molecular models.

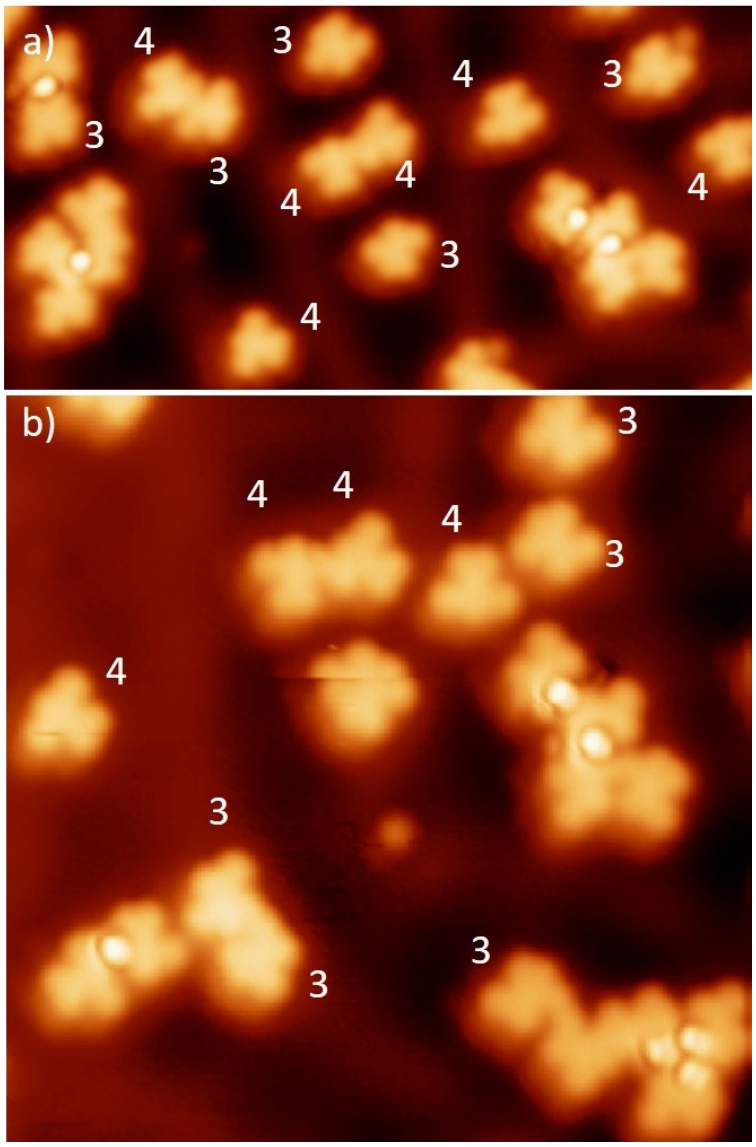

Fig. S3 Two randomly selected STM images to count the products **3** and **4,** for a sample prepared by direct deposition of molecule **1** on the Au(111) surface held at 350 ºC. We only mark the products which are easy to be identified. Ten monomers **3** and also ten monomers **4** are counted in the two STM images.

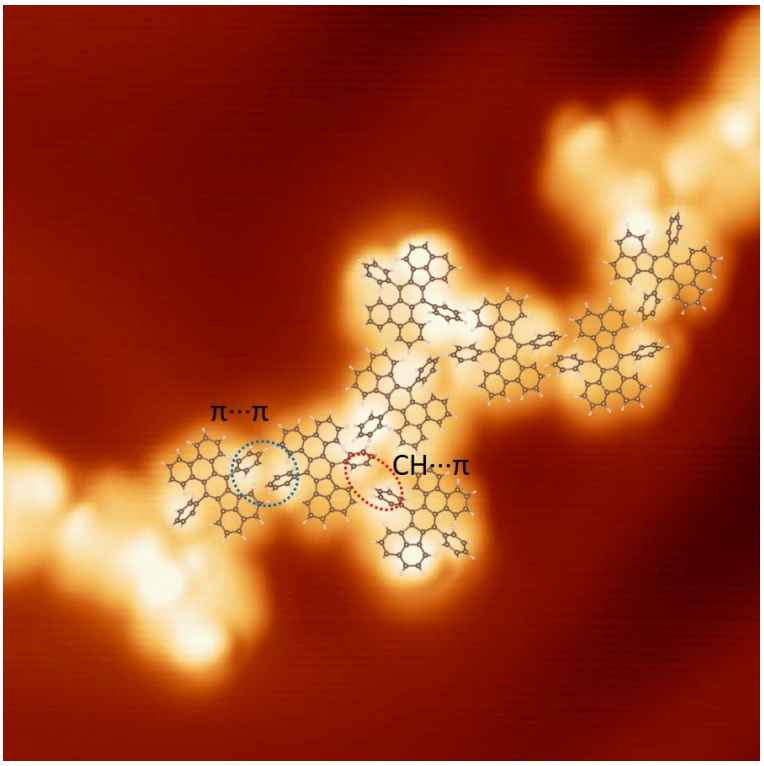

Fig. S4 STM image in Fig. 3b overlaid with the molecular models.

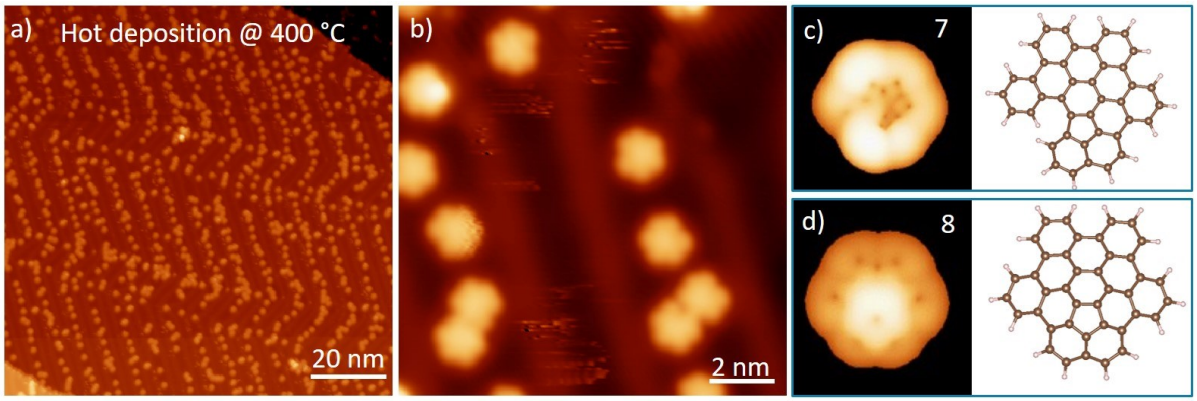

Fig. S5 Overview and magnified STM images of the sample by deposition of molecule **5** on Au(111) held at 400 °C. (c,d) Simulated STM image of products **7** and **8** (targeted product) shown in Scheme 1, along with the corresponding molecular models, respectively. It is obvious that the obtained monomer products in experiment are assigned to structure **7.**

Synthesis of the precursor molecules by solution chemistry

1. General methods

All reactions in solution were carried out under argon using oven-dried glassware. Thin layer chromatography was performed on Merck silica gel 60 F_{254} and the chromatograms were visualized with UV light (254 and 360 nm). Flash column chromatography was performed on Merck silica gel 60 (ASTM 230-400 mesh). ^{1}H and ^{13}C NMR spectra were recorded at 300 and 75 MHz or 500 and 125 MHz (Varian Mercury 300 or Bruker DPX-500 instruments), respectively. APCI spectra were determined on a Bruker Microtof instrument.

The synthesis of triflates **11** and **12** have been previously described.[1,2] Commercial reagents were purchased from ABCR GmbH or Aldrich Chemical Co. and were used without further purification. MeCN was purified by a MBraun SPS-800 Solvent Purification System. CsF was dried under vacuum at 100 ºC, cooled under argon and stored in a glove box. *n*-BuLi was used in hexane solution (2.4 M). *i*-Pr_2NH was dried by distillation over CaH_2.

2. Experimental details and spectroscopic data

2.1 Synthesis of cyclopentadienone 9

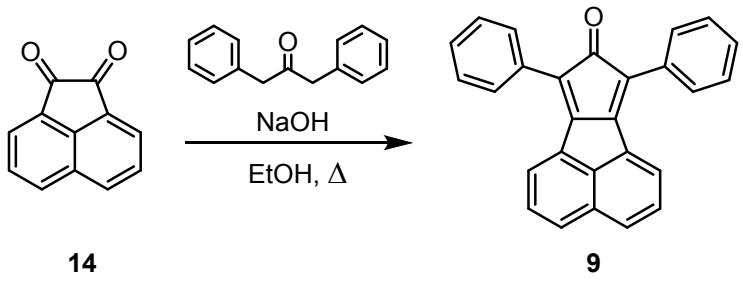

14 **9**

Fig. S6 Synthesis of compound **9**.

This synthetic protocol is based on a previously reported procedure.[3] A solution of NaOH (1.59 g) in EtOH (5 mL) was dropwise added at room temperature and under argon to a solution of acenaphthenequinone (**14**, 4.00 g, 22.0 mmol) and 1,3-diphenyl-2-propanone (5.32 g, 25.3 mmol) in EtOH (25 mL). The solution was stirred for 15 min at room temperature and refluxed for 30 min. Then, the reaction mixture was cooled to 0 °C and the resulting suspension was filtered to isolate a dark precipitate, which was subsequently washed with H_2O and EtOH to afford compound **9** (7.43 g, 95 %) as a dark solid.

^{1}H NMR (300 MHz, $CDCl_3$) δ: 8.06 (d, *J* = 7.1 Hz, 2H), 7.87 (d, *J* = 8.5 Hz, 2H), 7.85 – 7.78 (m, 4H), 7.59 (dd, *J* = 8.3, 7.2 Hz, 2H), 7.52 (ddd, *J* = 7.6, 6.9, 1.1 Hz, 4H), 7.46 – 7.37 (m, 2H) ppm. MS (APCI (M+1)) for $C_{27}H_{16}O$: 357.1

2.2 Synthesis of compound 1

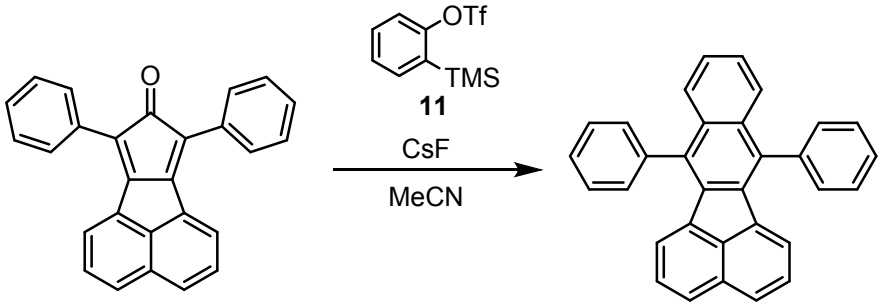

9 **1**

Fig. S7 Synthesis of compound **1**.

Anhydrous finely powdered CsF (767 mg, 5.05 mmol) was added to a solution of **9** (300 mg, 0.842 mmol) and triflate **11** (502 mg, 1.68 mmol) in MeCN (5 mL) and the mixture was stirred at room temperature under argon for 16 h. The reaction was quenched by the addition of H_2O (10 mL) and the aqueous phase was extracted with CH_2Cl_2 (2 x 10 mL). The combined organic phases were dried over anhydrous Na_2SO_4 and the solvent was evaporated under reduced pressure. The resulting mixture was purified by column chromatography (SiO_2, CH_2Cl_2:hexane, 1:4) to afford compound **1** (330 mg, 97%) as a yellow solid.
^{1}H NMR (300 MHz, $CDCl_3$) δ: 7.78 – 7.64 (m, 10H), 7.65 – 7.56 (m, 4H), 7.43 (dd, *J* = 6.4, 3.3 Hz, 2H), 7.36 (dd, *J* = 8.2, 7.1 Hz, 2H), 6.67 (d, *J* = 7.1 Hz, 2H) ppm. ^{13}C NMR (75 MHz, $CDCl_3$) δ: 139.01 (2xC), 136.71 (2xC), 135.70 (2xC), 135.02 (2xC), 134.89 (2xC), 132.99 (2xC), 130.14 (4xCH), 129.37 (4xCH), 128.07 (2xCH), 127.96 (2xCH), 126.90 (2xCH), 126.04 (2xCH), 125.88 (2xCH), 122.32 (2xCH) ppm. MS (APCI (M+1)) for $C_{32}H_{20}$: 405.1.

2.3 Synthesis of compound 5

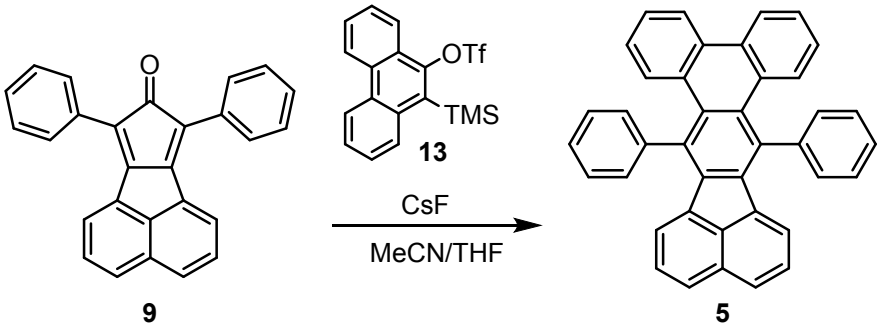

Fig. S8 Synthesis of compound **5**.

Anhydrous finely powdered CsF (447 mg, 2.94 mmol) was added to a solution of **9** (200 mg, 0.56 mmol) and triflate **13** (392 mg, 0.98 mmol) in a mixture of MeCN/THF (2:1, 9 mL), and the mixture was stirred at 55 ºC under argon for 16 h. Then, the solvents were evaporated under reduced pressure and the crude mixture was purified by column chromatography (SiO_2, CH_2Cl_2:hexane, 1:5) to afford compound **5** (244 mg, 86%) as a yellow solid.
^{1}H NMR (300 MHz, $CDCl_3$) δ: 8.46 (d, *J* = 8.3, 1.3 Hz, 2H), 7.89 (d, *J* = 8.1 Hz, 2H), 7.74 (d, *J* = 8.1 Hz, 2H), 7.62 (m, 10H), 7.42 (t, *J* = 7.6, 2H), 7.34 (t, *J* = 7.7 Hz, 2H), 7.07 (t, *J* = 7.5 Hz, 2H), 6.69 (d, *J* = 7.2 Hz, 2H) ppm. ^{13}C NMR (75 MHz, $CDCl_3$) δ: 142.78 (2C), 137.33 (C), 136.31 (C), 135.06 (C), 134.50 (C), 131.61 (C), 131.01 (2C), 130.74 (2CH), 129.78 (2CH), 129.31 (CH), 127.97 (CH), 127.60 (CH), 126.51 (CH), 126.42 (CH), 125.44 (CH), 123.61 (CH), 123.18 (CH) ppm. EM (APCI (M+1)) HR for $C_{40}H_{24}$ calcd: 505.1949, found: 519.1951.

3. ^{1}H and ^{13}C NMR spectra

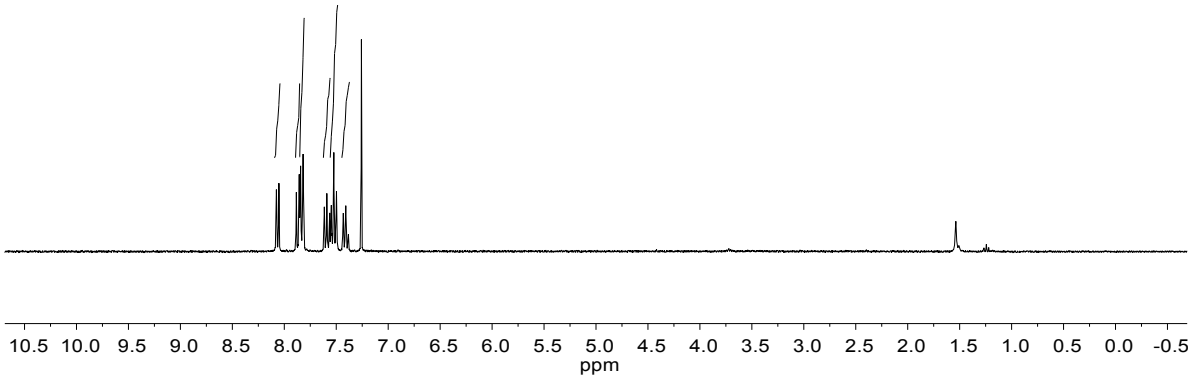

Fig. S9 ^{1}H NMR spectrum of compound **9**.

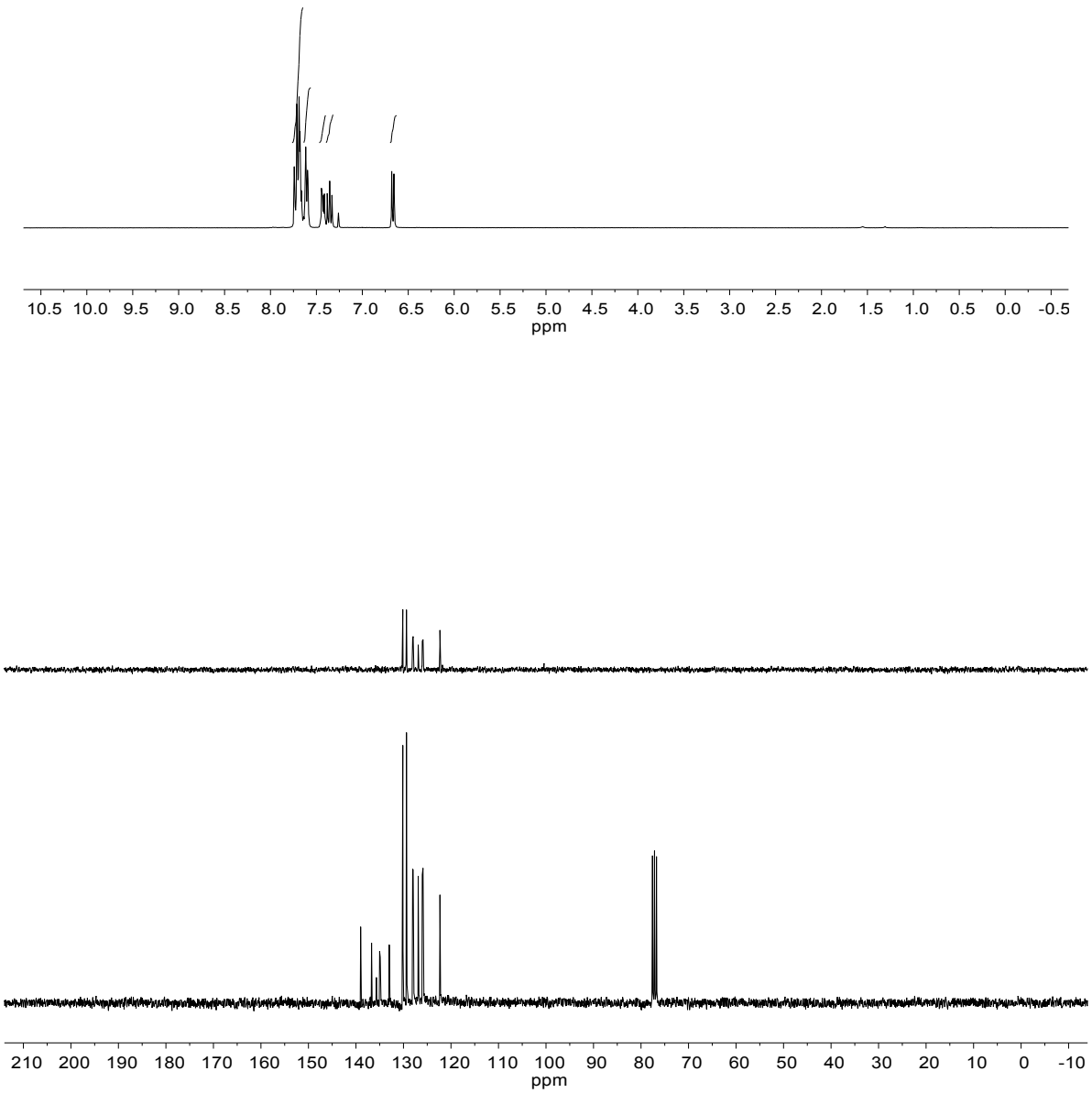

Fig. S10 ^{1}H NMR (top) and ^{13}C NMR (bottom) spectra of compound of compound **1**.

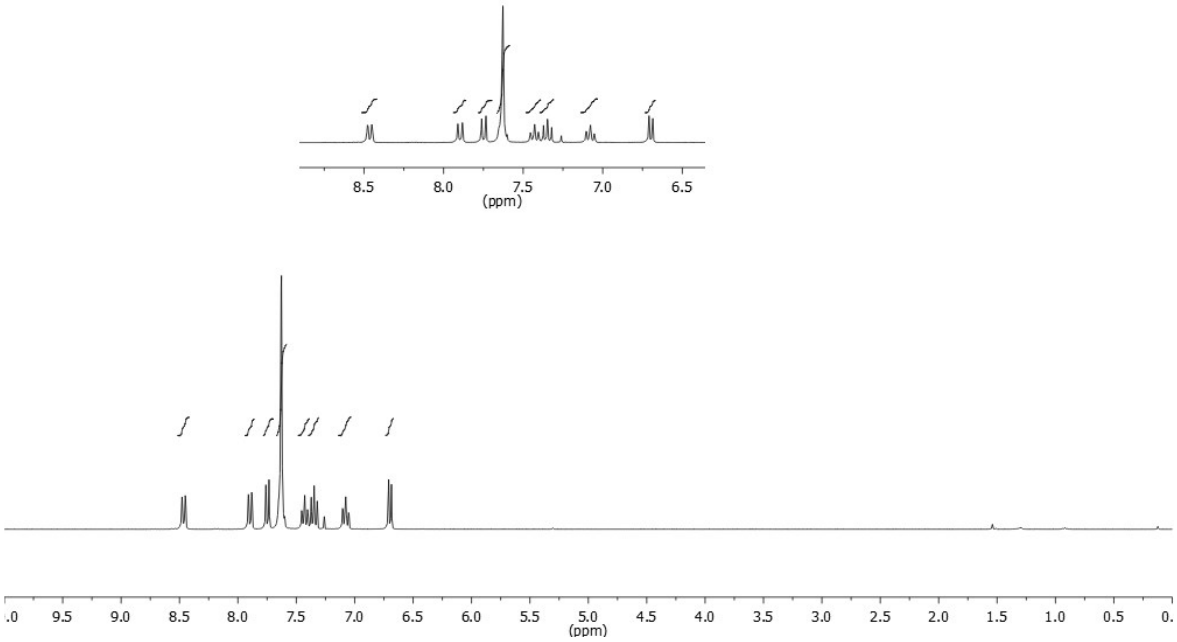

Fig. S11 ^{1}H NMR spectrum of compound of compound **5**.

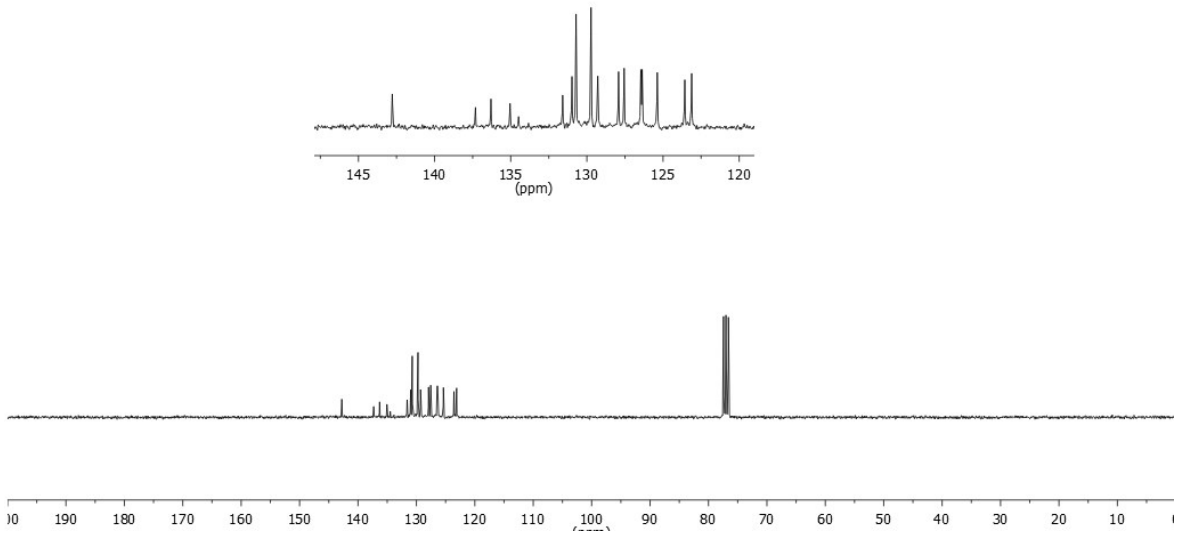

Fig. S12 ^{13}C NMR spectrum of compound of compound **5**.

Reference:

1 D. Peña, A. Cobas, D. Pérez and E. Guitián, *Synthesis*, 2002, **10**, 1454.
2 D. Peña, D. Pérez and E. Guitián, *J. Org. Chem*, 2000, **21**, 6944.
3 R. Vanel, F. Berthiol, B. Bessières and C. Einhorn, J., *Synlett*, 2011, **9**, 1293.